

**De novo fabrication of multi-heteroatoms-doped carbonaceous materials via an in situ doping strategy**

Journal:	<i>Journal of Materials Chemistry A</i>
Manuscript ID	TA-COM-12-2019-013586.R1
Article Type:	Communication
Date Submitted by the Author:	03-Feb-2020
Complete List of Authors:	Luo, Yali; Nanjing Tech University, College of Materials Science and Engineering Yang, Zhenzhen; The University of Tennessee, Chemistry Guo, Wei; The University of Tennessee Chen, Hao; The University of Tennessee, Department of Chemistry Wang, Tao; University of Tennessee Knoxville, Liu, Yunfei; Nanjing Tech University, College of Materials Science and Engineering Lu, Yinong; Nanjing Tech University, College of Materials Science and Engineering Luo, Huimin; Oak Ridge National Laboratory, Energy and Transportation Science Dai, Sheng; Oak Ridge National Laboratory,

COMMUNICATION

De novo fabrication of multi-heteroatoms-doped carbonaceous materials via an in situ doping strategy

Received 00th January 20xx,
Accepted 00th January 20xx

Yali Luo,^a Zhenzhen Yang,^{*b,c} Wei Guo,^b Hao Chen,^b Tao Wang,^b Yunfei Liu,^a Yinong Lyu,^a Huimin Luo,^c and Sheng Dai,^{*b,c}

DOI: 10.1039/x0xx00000x

Finding a succinct strategy by which to fabricate multi-heteroatom-doped nanoporous carbonaceous materials is a long-term challenge and highly desired research topic. Key to success is the rational design of easily obtained and functionalized precursors. Herein, de novo fabrication of multi-heteroatom-doped carbonaceous materials, including boron, nitrogen, oxygen, fluorine, and sulfur, was achieved via a one-step in situ doping procedure using task-specific ionic liquids (TSILs) as precursors. Our strategy hinges on the adoption of particularly designed TSILs with structures functionalized by (1) boron source-containing anions, (2) imidazolium functionalities as carbon and nitrogen source, (3) nitrile groups capable of trimerization during the heating process, and (4) bis(trifluoromethanesulfonyl)imide and related anions performing as the source for heteroatoms (i.e., fluorine, nitrogen, sulfur, and oxygen) and porogen. The unique structures of the as-prepared TSILs endow them as qualified precursors for the production of multi-heteroatom-doped carbonaceous materials through simple thermal treatment, with surface areas up to 1021 m² g⁻¹. The introduction of multiple heteroatoms renders the carbonaceous materials with efficient adsorption performance for the capture of hazardous anionic pollutants, dyes, and neutral organic molecules. This finding expands the versatility of TSILs with multi functionalized architectures, delivering nanoporous materials with wide applications.

Introduction

Design and application of carbonaceous materials are at the forefront of material chemistry as they are ubiquitous in various technological and energy-related fields.¹⁻³ The unique properties—for example, high specific surface area,

controllable porous structure, various morphologies, and excellent chemical, mechanical, and thermal stability—make them promising candidates in adsorption/separations,⁴ catalysis,⁵ and energy storage/conversion.⁶ Generally, technologies for carbonaceous material fabrication are mainly included as thermal treatment of organic compounds or polymers, hard and soft template-involved synthesis, and chemical and physical activation pathways.⁷ Comparatively, direct carbonization is demonstrated to be very efficient, and various precursors can be used as the carbon source, including fossil/biomass-derived materials,⁸⁻¹⁰ pre-synthesized organic polymers,^{11, 12} and metal-organic frameworks (MOFs).¹³ However, the low-vapor-pressure properties of organic compound precursors make them prone to evaporate or decompose to gaseous products during high-temperature treatment, leading to low carbon yields. The carbonization of organic polymers or MOFs avoids this issue, but the complicated and tedious synthetic procedures prior to carbonization limit their practical applications.^{14, 15} An alternative procedure combining the merits of the above-mentioned processes involves adopting ionic liquids (ILs) as starting materials.¹⁶⁻¹⁹ ILs are entirely composed of ion pairs and characterized by many unique properties, such as negligible volatility, high thermal stability, molecular tunability, and carbon-rich nature.¹⁹⁻²¹ These properties create the possibilities of designing functionalized carbonaceous materials with adjustable chemical and electric properties considering the tremendous cation/anion structures in task-specific ionic liquids (TSIL) endowed by organic synthetic chemistry.

On the other hand, surface charge properties exhibited by carbonaceous materials can be tuned by heteroatom doping.¹ The introduction of heteroatoms such as boron, nitrogen, sulfur, and phosphorus to replace some of the carbon atoms could cause electron modulation due to their different electronegativity, leading to improved optoelectronic properties and/or defect-induced chemical functionalities.^{22, 23} In general, heteroatom-doped carbonaceous materials can be prepared either by in situ doping during preparation or post-

^a College of Materials Science and Engineering, Nanjing Tech University, Nanjing, 211816, PR China.

^b Department of Chemistry, The University of Tennessee, Knoxville, TN, 37996, USA. Email: ZYANG17@utk.edu; dais@ornl.gov.

^c Chemical Sciences Division, Oak Ridge National Laboratory, Oak Ridge, TN 37831, USA.

Electronic Supplementary Information (ESI) available: [experimental details, supplementary table and figures]. See DOI: 10.1039/x0xx00000x

COMMUNICATION

Journal Name

treatment of the as-prepared carbon nanomaterials with heteroatom-containing precursors. Nanodiamond-based carbon material with the electron-rich nitrogen and electron-deficient boron co-doped on the surface was prepared, exhibiting high catalytic efficiency as heterogeneous metal-free catalysts for hydrogenation.²⁴ The materials were fabricated through high-temperature treatment of ultradispersed nanodiamond coated with a boron- and nitrogen-containing IL (i.e., 1-butyl-3-methylimidazolium tetrafluoroborate). Three-dimensional porous carbon networks co-doped with nitrogen and phosphorus prepared by pyrolysis of a supermolecular aggregate of self-assembled melamine, phytic acid, and graphene oxide worked well as efficient metal-free bifunctional catalysts for oxygen reduction and hydrogen evolution reactions.²³ Comparatively, the post-treatment procedure often leads only to surface functionalization without altering their bulk properties, whereas the in situ doping of heteroatoms can help to homogeneously incorporate the heteroatoms into the entire nanoporous carbon matrix.¹ Notably, TSILs have exhibited good performance in producing heteroatom-doped carbonaceous materials with enhanced performance via direct introduction of heteroatoms (e.g., nitrogen and sulfur) in the cationic or anionic backbones. For example, nitrogen-doped carbonaceous materials could be fabricated using nitrile group-functionalized TSILs^{17, 21, 25-27} and protic ILs synthesized via a straightforward neutralization between amines and strong acids.^{28, 29} Furthermore, nitrogen- and sulfur-doped hierarchically porous carbon materials were prepared using protic ILs with a HSO_4^- anion toward supercapacitive energy storage.^{29, 30} Although the subject of carbonaceous materials fabrication with TSILs as precursors has been extensively studied up to now, the doped heteroatoms are still limited and fabrication of multi-heteroatom-doped nanoporous carbon is rarely reported. Keys to success include rational design of the TSIL precursors to involve heteroatoms within the cation/anion and functionalities capable of polymerization during thermal treatment. Therefore, despite significant challenges, the development of a novel and simple fabrication pathway for multi-heteroatom-doped carbonaceous materials would propel further advancement in this field.

Herein, de novo fabrication of multi-heteroatom-doped carbonaceous materials, including boron, nitrogen, oxygen, fluorine, and sulfur, was achieved via a one-step in situ doping procedure using TSILs as precursors (Fig. 1). Our strategy hinges on the adoption of particularly designed TSILs with structures functionalized by (1) boron source-containing anions, (2) imidazolium functionalities as carbon and nitrogen source, (3) nitrile groups capable of trimerization during the heating process, and (4) bis(trifluoromethanesulfonyl)imide and related anions performing as the source for heteroatoms (i.e., fluorine, nitrogen, sulfur, and oxygen) and porogen. The unique structures of the as-prepared TSILs endow them as qualified precursors for the production of multi-heteroatom-doped carbonaceous materials through simple thermal treatment, with surface areas up to $1,021 \text{ m}^2 \text{ g}^{-1}$ and the total pore volume of $0.50 \text{ cm}^3 \text{ g}^{-1}$. Notably, the resultant materials performed well in CO_2 adsorption with uptake capacities reaching 3.96 mmol g^{-1}

at 1 bar and 273 K. In addition, the introduction of multiple heteroatoms also renders the carbonaceous materials with efficient adsorption performance for the capture of hazardous anionic pollutants, dyes and neutral organic molecules. This finding expands the versatility of TSILs with multifunctionalized architectures, affording nanoporous materials with wide applications.



Fig. 1 Structures of the TSIL precursors, $\text{Na}[(\text{BIm}_4\text{-CH}_2\text{CN})_4(\text{TFSI})_4]$ and $\text{Na}[(\text{BIm}_4\text{-CH}_2\text{CN})_4(\text{BETI})_4]$, and synthetic procedure for the production of multi-heteroatom-doped carbonaceous materials, BNOFS-C-1 and BNOFS-C-2.

Results and discussion

The synthetic pathway and the molecular structures of the TSIL precursors used in this work, including $\text{Na}[(\text{BIm}_4\text{-CH}_2\text{CN})_4(\text{TFSI})_4]$ and $\text{Na}[(\text{BIm}_4\text{-CH}_2\text{CN})_4(\text{BETI})_4]$, are shown in Fig. 1. First, sodium tetrakis-(3-cyanomethyl-1-imidazolyl)borate chloride ($\text{Na}[(\text{BIm}_4\text{-CH}_2\text{CN})_4\text{Cl}_4]$) was synthesized by a quaternization reaction.¹⁷ Then, sodium tetrakis-(3-cyanomethyl-1-imidazolyl)borate bis(trifluoromethanesulfonyl)imide ($\text{Na}[(\text{BIm}_4\text{-CH}_2\text{CN})_4(\text{TFSI})_4]$) and sodium tetrakis-(3-cyanomethyl-1-imidazolyl)borate bis(pentafluoroethylsulfonyl)imide ($\text{Na}[(\text{BIm}_4\text{-CH}_2\text{CN})_4(\text{BETI})_4]$) were prepared using the corresponding lithium salts through a simple anion exchange method (for synthetic details and characterization, see the Electronic Supplementary Information). The chemical structure of TSIL precursors was characterized by fourier transform infrared spectroscopy (FTIR) and nuclear magnetic resonance (see Figs. S1-S4 for details). Subsequently, ionothermal treatment of the as-prepared TSILs was conducted to produce the heteroatom-doped carbonaceous materials, and the resultant materials were denoted as BNOFS-C-1 (for carbons from $\text{Na}[(\text{BIm}_4\text{-CH}_2\text{CN})_4(\text{TFSI})_4]$) and BNOFS-C-2 (for carbons from $\text{Na}[(\text{BIm}_4\text{-CH}_2\text{CN})_4(\text{BETI})_4]$), respectively.

Thermal gravimetric analysis (TGA) of the TSIL precursors was conducted to investigate their thermal properties. As can be seen from the TGA profiles (Fig. S5), decomposition of $\text{Na}[(\text{BIm}_4\text{-CH}_2\text{CN})_4(\text{TFSI})_4]$ and $\text{Na}[(\text{BIm}_4\text{-CH}_2\text{CN})_4(\text{BETI})_4]$ began at about 300°C and 350°C , respectively. At 400°C , the weight loss of $\text{Na}[(\text{BIm}_4\text{-CH}_2\text{CN})_4(\text{TFSI})_4]$ and $\text{Na}[(\text{BIm}_4\text{-CH}_2\text{CN})_4(\text{BETI})_4]$ achieved about 67 wt% and 45 wt%, respectively. The carbonization process was almost completed at about 470°C for both TSIL precursors. As previously reported, nitrile-functionalized ILs can polymerize at high temperature, forming

triazine units through trimerization reactions between nitrile groups.³¹ When $\text{Na}[(\text{BIm}_4\text{-CH}_2\text{CN})_4(\text{TFSI})_4]$ and $\text{Na}[(\text{BIm}_4\text{-CH}_2\text{CN})_4(\text{BETI})_4]$ are pyrolyzed at 600 °C, polymerization and carbonization reactions take place, and black powder is obtained (Fig. 1). In the FT-IR spectrum of BNOFS-C-1 obtained at 400 °C (Fig. S7), the existence of triazine units is characterized by two strong absorption bands at 1520 and 1336 cm^{-1} corresponding to the aromatic C-N stretching and breathing modes in the triazine unit, respectively, together with the characteristic peak for C=N located at 1592 cm^{-1} .³² This verified that successful polymerization of $\text{Na}[(\text{BIm}_4\text{-CH}_2\text{CN})_4(\text{TFSI})_4]$ was realized through the trimerization of nitrile groups, leading to formation of triazine frameworks by thermal treatment. However, the characteristic peaks for triazine units became pretty weak in BNOFS-C-1 obtained at higher pyrolysis temperatures (600 °C and 800 °C), indicating the rearrangement of the skeleton and partial cleavage of the triazine units at high temperature. Reduced intensity of the signal for triazine units has also been observed in the FTIR spectrum of BNOFS-C-2 obtained at 600 °C (Fig. S8). The carbons obtained at 600 °C (BNFSO-C-1 and BNFSO-C-2) were selected as typical samples for structure analysis. A proposed carbon formation process was shown in Fig. S6. The surface elemental composition and chemical state of heteroatoms of BNFSO-C-1 and BNFSO-C-2 are evaluated by and x-ray photoelectron spectroscopy (XPS) spectra. As shown in Figs. 2a and S5a, the XPS survey spectra confirmed the presence of five heteroatoms, including boron, nitrogen, oxygen, fluorine, and sulfur within the backbone of the carbonaceous materials, indicating the successful introduction of multiple heteroatoms through the in situ doping strategy. The oxidation states of carbon and other heteroatoms within the carbonaceous materials are investigated with high resolution spectra of the corresponding atoms (Fig. 2c–h). The C1s spectrum can be deconvoluted into three peaks with binding energies at 284.8, 286.1, and 287.8 eV, which are assigned to the aromatic C-C, C=N, and C-F, respectively (Fig. 2c). It should be noted that BNOFS-C-1 also contains a small amount of boron (0.8 at.%) (Fig. 2b). The characteristic peak of B1s is detected at 192.1 eV, which is attributed to the presence of a B-N bond (Fig. 2d). In Fig. 2e, the high-resolution XPS spectrum of N1s is resolved into three strong peaks corresponding to pyridinic-N (398.6 eV), pyrrolic-N (400.5 eV), and N-B bond (402.5 eV).³³ Although the $(\text{TFSI})_4^-$ and $(\text{BETI})_4^-$ anions acted as porogen and partially decomposed to volatile products during pyrolysis,¹⁶ the oxygen, sulfur, and fluorine were successfully doped into the carbonaceous materials. The O1s peak can be resolved into two compositions with binding energies of 532.1 eV and 533.5 eV; the former corresponds to the C=O and the latter to the C-O (Fig. 2f). The two distinct peaks at 686.4 eV and 687.4 eV in Fig. 2g correspond to the semi-ionic, covalent C-F bonds originating from $(\text{TFSI})_4^-$ anions. Peaks for S2p are observed at 164.1 eV and 170.9 eV, which correspond to C-S and S-O species, respectively (Fig. 2h).³⁴⁻³⁶ The XPS results of BNOFS-C-2 are presented in Fig. S9, indicating the involvement of multiple heteroatoms with the structural skeleton. Elemental analysis was conducted to further confirm the composition of the carbonaceous materials. Notably, the fluorine content in

BNOFS-C-1 and BNOFS-C-2 is 1.18 wt% and 2.28 wt%, respectively. These values are much lower than that detected by XPS, indicating F is mainly distributed on the surface of the carbonaceous materials.

Raman spectra of both BNFSO-C-1 and BNFSO-C-2 presented two first-order Raman bands for disordered carbons (D band, 1345 cm^{-1}) and graphitic carbons (G band, 1572 cm^{-1}) (Fig. S10). For both materials, the I_D/I_G ratio is about 0.98, signifying the similar graphitization degree in the carbon structures. Fig. S11 displayed the X-ray diffraction (XRD) patterns of the as-synthesized carbon materials. Both BNFSO-C-1 and BNFSO-C-2 showed two broad diffractions centered at 25° and 43°, corresponding to the graphite (002) and (101) planes, which also indicated the low crystallinity and the amorphous characteristics of the samples.

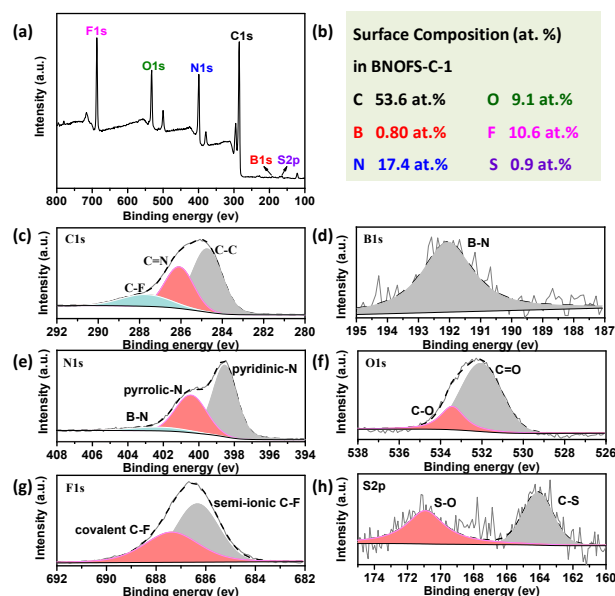


Fig. 2 XPS spectra of BNFSO-C-1. (a) XPS survey spectrum; (b) Surface composition of the elements; (c–h) spectrum of C1s, B1s, N1s, O1s, F1s, and S2p, respectively.

The morphology, microstructure, and composition of the porous carbons were further investigated by scanning electron microscopy (SEM) and transmission electron microscopy (TEM) (Figs. 3a–3d). SEM images (Figs. 3a and 3b) demonstrated that BNOFS-C-1 consisted of irregular, small nanoparticles. TEM images (Figs. 3c and 3d) showed the presence of layered porous carbon nanosheets as well as small pores within the architecture. However, the pores were irregularly arranged, indicating the amorphous architecture of the carbonaceous material. The corresponding chemical mappings are displayed in Figs. 3e and S12. As can be seen, the heteroatoms (i.e., boron, fluorine, nitrogen, oxygen, and sulfur) were evenly distributed within the carbon frameworks.

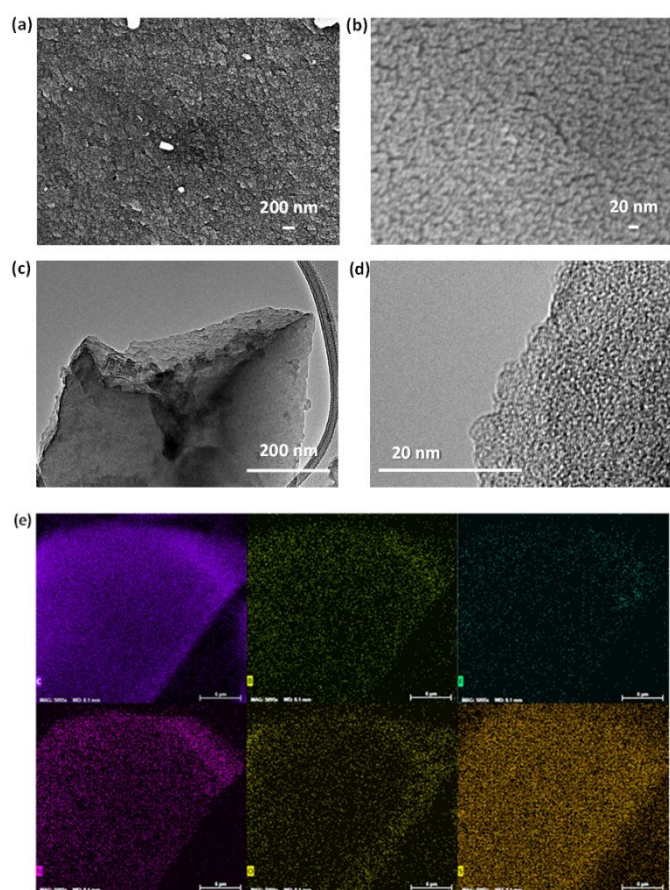


Fig. 3 (a, b) SEM, (c, d) TEM images and (e) the corresponding chemical mappings of BNOFS-C-1 (scale bar: 6 μm).

The porous properties of both carbonaceous materials were analyzed by nitrogen sorption measurement at 77 K. As seen in Fig. 4a, both BNOFS-C-1 and BNOFS-C-2 exhibit reversible type I isotherms with a sharp uptake at low relative pressure ($P/P_0 < 0.15$), indicating that both carbonaceous materials have extensive micropore structure. Notably, the anion structures of the TSIL precursors have a profound influence on the surface area. Carbonaceous material derived from larger anions shows higher surface area and pore volume. For instance, simply replacing $(\text{TFSI})_4^-$ with $(\text{BETI})_4^-$ for a fixed cation results in increased BET surface areas, from $594 \text{ m}^2 \text{ g}^{-1}$ (BNOFS-C-1) to $1,021 \text{ m}^2 \text{ g}^{-1}$ (BNOFS-C-2) (Figs. S13 and S14). This may be due to the templating role of the anion during the carbonation process. Besides the anion structures, the carbonization temperature also has a profound influence on the resulting surface areas. With the low carbonization temperature of 400°C , the obtained sample BNOFS-C-1(400) is nonporous carbon, probably owing to the involvement of the counterion $[\text{TFSI}]^-$ within the network. However, polymerization of $\text{Na}[(\text{BIm}_4\text{-CH}_2\text{CN})_4(\text{TFSI})_4]$ at 800°C led to carbon material with a lower surface area (BNOFS-C-1(800), $540 \text{ m}^2 \text{ g}^{-1}$) than that obtained by carbonization at 600°C (BNOFS-C-1, $594 \text{ m}^2 \text{ g}^{-1}$) (Fig. S15). This may be due to further decomposition and collapse of the micropore structures within the skeleton by thermal treatment at high temperature (800°C).³¹ The contribution of microporosity to the networks can be calculated as the ratio of

the micropore volume (V_{micro}) to the total pore volume (V_{total}). According to Table S1, the microporosities of BNOFS-C-1 and BNOFS-C-2 are $\sim 46\%$ and $\sim 50\%$, respectively. The results agree well with the shape of the nitrogen isotherms and reveal a mainly microporous network structure for both carbonaceous materials. The pore size distributions analyzed using nonlocal density functional theory (NLDFT) further confirm the microporous nature of the materials (Fig. 4b). Both BNOFS-C-1 and BNOFS-C-2 display main pore size distribution below 2 nm. In addition, there are more ultramicropores ($\sim 0.55 \text{ nm}$) than larger micropores in both carbonaceous materials. In order to further investigate the ultramicropores of the porous carbon, argon sorption isotherms were also collected at 87 K (Fig. S16a). Again, the sorption isotherms of BNOFS-C-1 showed a typical type-I behavior with the BET surface area of $644 \text{ m}^2 \text{ g}^{-1}$. This value is slightly higher than that of N_2 adsorption. Pore size distribution was estimated by fitting the argon uptake branch with NLDFT and found to exhibit three major pore size distributions centered at 0.51, 0.77, and 1.14 nm for the carbon material (Fig. S16b). These ultramicropores may arise from the cleavage of C-F bonds during carbonization. These pore characteristics put both carbonaceous materials in the same league as well-known microporous skeletons with high surface areas (e.g., zeolites, MOFs, and porous organic polymers).^{37, 38}

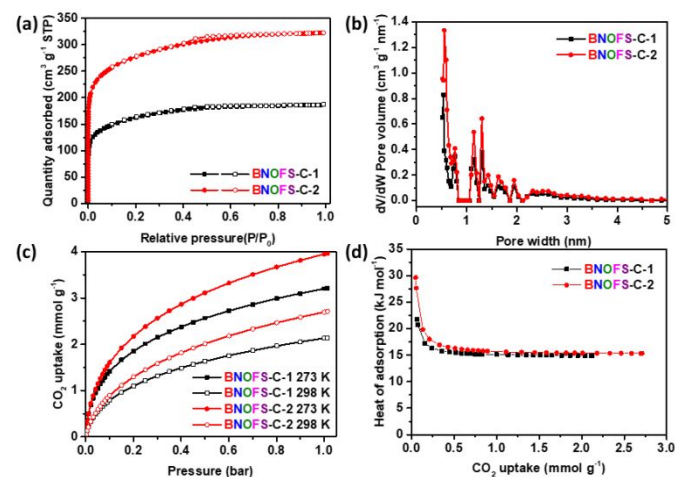


Fig. 4 Characterization and CO_2 uptake performance of BNOFS-C-1 and BNOFS-C-2. (a) N_2 sorption isotherms, (b) pore size distribution, (c) CO_2 adsorption isotherms, and (d) isosteric heats of adsorption (Q_{st}).

The CO_2 adsorption performance of the carbonaceous materials is assessed by CO_2 sorption isotherms at 273 K and 298 K. As shown in Fig. 4c, the CO_2 uptake capacity increases with an increase in the specific surface area. BNOFS-C-2 possessing the higher BET-specific surface area exhibits the higher CO_2 uptake of 3.96 mmol g^{-1} at 1.0 bar and 273 K. This value is superior or comparable to other ILs and salts-derived porous carbon materials.¹⁶ In addition, no saturation is observed up to 1 atm, suggesting that a higher CO_2 uptake capacity could be achieved at a higher pressure. At the low pressure of 0.15 bar, both BNOFS-C-1 and BNOFS-C-2 exhibit high CO_2 uptake capacities of 1.66 mmol g^{-1} and 1.92 mmol g^{-1} at 273 K, respectively. These values are still higher than most reported porous carbons for

CO₂ capture under identical conditions.¹⁶ Such high CO₂ sorption capability may be due to the high nitrogen and fluorine content in the carbon networks.³⁹ In addition, the significant amount of ultramicropores also offers high CO₂ adsorption potential. For comparison, previous reported porous carbon with less heteroatoms, e.g., carbon-derived from 1,3-bis(cyanomethyl)imidazolium bis(trifluoromethanesulfonyl)imide ([BCNIm][TFSI]),¹⁷ was also synthesized and the CO₂ sorption isotherm was measured. At 273 K, porous derived from [BCNIm][TFSI] has a CO₂ uptake of 2.99 mmol g⁻¹, which was much lower than that of BNOFS-C-1 and BNOFS-C-2 (Table S2). The isosteric heat of adsorption (Q_{st}) for BNOFS-C-1 and BNOFS-C-2 was calculated using the Clausius-Clapeyron method from the CO₂ isotherms collected at 273 K and 298 K (Fig. 4d). At zero coverage, the Q_{st} of BNOFS-C-1 and BNOFS-C-2 for CO₂ is found to be 21.7 kJ mol⁻¹ and 29.6 kJ mol⁻¹, respectively. These values are relatively larger than that of active carbon (5.8 kJ mol⁻¹),⁴⁰ but lower than those of functionalized microporous polymers with CO₂-philic functionalities, such as triazine polyimides (29.2–34.4 kJ mol⁻¹),⁴¹ CMP-1-COOH (33 kJ mol⁻¹),⁴² polyimine (PI-1, 34 kJ mol⁻¹),⁴³ PPN-6-SO₃Li (35.7 kJ mol⁻¹),⁴⁴ polyindole fiber (PIF6, 42.7 kJ mol⁻¹),⁴⁵ and polycarbazole (45 kJ mol⁻¹).⁴⁶ Furthermore, the BNOFS-C-1 has exhibited high stability during the CO₂ uptake process, with no significant changes being observed within five consecutive CO₂ adsorption cycles both at 273 and 298 K (Fig. S17). The introduction of heteroatoms into porous carbon not only enhanced the CO₂ uptake capacity but also led to more preferential adsorption of CO₂ over N₂. The N₂ adsorption isotherms at 273 and 298 K for BNOFS-C-1 are shown in Fig. S18. Using ideal adsorption solution theory (IAST) for CO₂:N₂ (0.15:0.85), the CO₂/N₂ selectivity was predicted to be 29 and 16 at 273 and 298 K respectively for BNOFS-C-1. These values are much higher than that of other previously reported porous carbons such as NDPCs (9.7~20.8),⁴⁷ NETs (10.6~22.5)⁴⁸ and MOP-Cs (6~21)¹⁵ at 1 bar and 273 K.

Recently, the utilization of microporous materials for direct separation and adsorption of organic molecules from water has attracted extensive research interest.⁴⁹ It has been reported that the heteroatom-enriched porous network is highly electronegative and might provide powerful adsorption sites to attract chemical molecules such as dyes.⁵⁰ With their high surface areas, rich micropores structure, and multi-heteroatom doping, BNOFS-C-1 and BNOFS-C-2 could be used as adsorbents for removal of dyes in water. Methylene blue (MB), an organic cationic dye with molecular size of 17.0 × 7.6 × 3.3 Å, is considered the primary source of pollution in water bodies. Utilization of various materials for MB adsorption has been reported;⁵¹⁻⁵³ however, MB adsorption by multi-heteroatom-doped porous carbon is scarce. Figs. 5a and 5b show the absorption spectra at different time intervals of MB aqueous solution treated with BNOFS-C-1 and BNOFS-C-2, respectively. As the MB adsorption proceeds, the characteristic band of MB becomes increasingly weaker. As shown in Fig. 5c, more than 99% of MB could be removed from water within 40 min at room temperature. Especially for BNOFS-C-1, MB was completely removed in only 10 min. Although both carbonaceous materials

have similar chemical structures and the surface area of BNOFS-C-1 is slightly smaller than that of BNOFS-C-2, the faster MB uptake rate of BNOFS-C-1 was probably due to its higher heteroatom content within the architecture, exposing more active sites to form hydrogen bonds with MB during the adsorption process. This can be confirmed by the relatively slow MB adsorption kinetic of [BCNIm][TFSI]-derived porous carbon and other porous carbons with less heteroatoms (Fig. S19 and Table S2). It should be noted, however, the maximum MB adsorption capacity of the porous carbons is still proportional to their respective BET surface areas. The maximum MB adsorption capacity was 46 mg g⁻¹ and 123 mg g⁻¹ for BNOFS-C-1 and BNOFS-C-2, respectively (Fig. S20a and b). Besides the cationic dye MB, BNOFS-C-1 also showed good adsorption ability with anionic MnO₄⁻ and uncharged 4-nitrophenol (4-NP) (Figs. 5e and 5f). Almost 80% of the MnO₄⁻ ion was removed within 60 min, while for uncharged 4-NP, within only 20 minutes. Further, capacity of BNOFS-C-1 for MnO₄⁻ ion was calculated to be 289 mg g⁻¹, which can be counted as one of the highest values in the regime of porous material (Fig. S20c and Table S2). It was reported that the diameters of MnO₄⁻ and 4-NP are less than 10 Å.^{49,53} Considering the pore size distribution of BNOFS-C-1, we could speculate that the MnO₄⁻ ion and 4-NP molecule could not only be adsorbed into the micropores but also into the mesoporous. Moreover, heteroatoms (i.e., N, O, F, and S) in BNOFS-1 also play critical roles in the adsorption of these oxo-anion or dye molecules. These results indicate the versatility of the porous carbon in dye adsorption thanks to the simultaneous presence of nanoporous architecture and multiple hetero atoms within the backbone.

Conclusions

In summary, rational design of TSILs including multiple cations and anions within the structure was realized. With resultant TSIL precursors, multi-heteroatom-doped carbonaceous materials, including boron, nitrogen, oxygen, fluorine, and sulfur, were fabricated through simple ionothermal treatment. Nanoporous carbonaceous materials were obtained in the absence of additional porogen with large surface areas. Unique structures of the as-prepared carbons render them as efficient adsorbents with high CO₂ uptake capacity. In addition, synergistic improvement induced by the nanopores and heteroatom doping makes the carbons promising candidates for the adsorption of dyes including cationic, anionic and neutral ones. The strategy developed in this work unlocks new opportunities for designing novel functionalized carbonaceous materials and extending their applications.

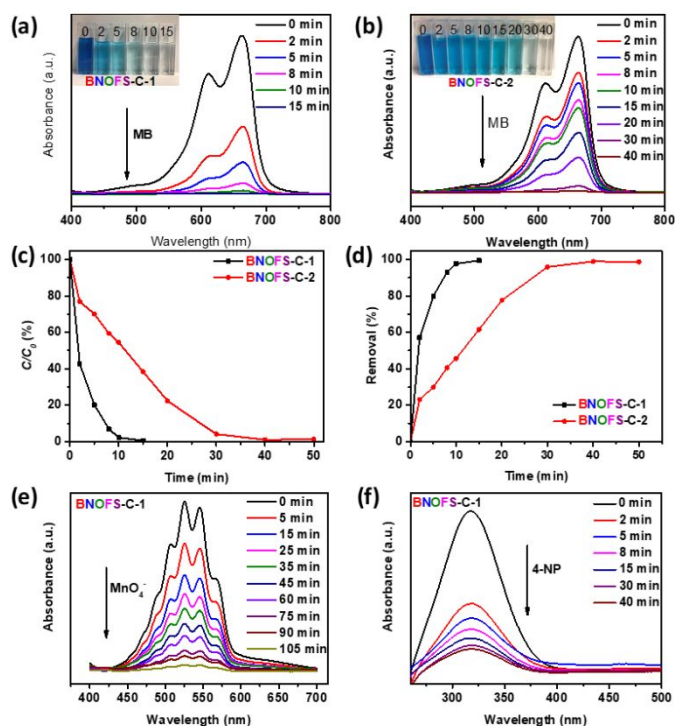


Fig. 5 Ultraviolet-visible absorption (UV-Vis) spectra of MB aqueous solution treated with (a) BNOFS-C-1 and (b) BNOFS-C-2 at different time intervals. The inset photograph shows the corresponding color change of the MB solution. (c) The adsorption rates of MB. (d) Removal of MB at different time intervals. (e) UV-Vis spectra of MnO₄⁻ and (f) 4-NP solutions at different time intervals using BNOFS-C-1 as adsorbent. The initial concentrations of the MB, MnO₄⁻, and 4-NP solutions are 0.05 mM, 0.5 mM, and 0.05 mM, respectively.

Acknowledgments

The research was supported by the Division of Chemical Sciences, Geosciences, and Biosciences, Office of Basic Energy Sciences, US Department of Energy, and the Jiangsu Overseas Visiting Scholar Program for University Prominent Young & Middle-aged Teachers, China.

Conflicts of interest

There are no conflicts to declare.

Notes and references

- M. R. Benzigar, S. N. Talapaneni, S. Joseph, K. Ramadass, G. Singh, J. Scaranto, U. Ravon, K. Al-Bahily and A. Vinu, *Chem. Soc. Rev.*, 2018, **47**, 2680-2721.
- W. Yang, X. Li, Y. Li, R. Zhu and H. Pang, *Adv. Mater.*, 2019, **31**, 1804740-1804775.
- Z. Chang, Y. Yang, J. He and J. F. Rusling, *Dalton Trans.*, 2018, **47**, 14139-14152.
- G. Durá, V. L. Budarin, J. A. Castro-Osma, P. S. Shuttleworth, S. C. Z. Quek, J. H. Clark and M. North, *Angew. Chem.-Int. Edit.*, 2016, **55**, 9173-9177.
- B. Qiu, M. Xing and J. Zhang, *Chem. Soc. Rev.*, 2018, **47**, 2165-2216.
- J. Zhang and L. Dai, *Angew. Chem.-Int. Edit.*, 2016, **55**, 13296-13300.
- P. Zhang, Z.-A. Qiao and S. Dai, *Chem. Commun.*, 2015, **51**, 9246-9256.
- S. Dutta, A. Bhaumik and K. C. W. Wu, *Energy Environ. Sci.*, 2014, **7**, 3574-3592.
- M. Danish and T. Ahmad, *Renew. Sust. Energ. Rev.*, 2018, **87**, 1-21.
- P. Li, J. Liu, Y. Wang, Y. Liu, X. Wang, K.-W. Nam, Y.-M. Kang, M. Wu and J. Qiu, *Chem. Eng. J.*, 2016, **286**, 632-639.
- J.-S. M. Lee, M. E. Briggs, T. Hasell and A. I. Cooper, *Adv. Mater.*, 2016, **28**, 9804-9810.
- P. Li, T. Shi, D. Yao, Y. Wang, C. Liu and Y. Zheng, *Carbon*, 2016, **110**, 87-96.
- K. Shen, X. Chen, J. Chen and Y. Li, *ACS Catal.*, 2016, **6**, 5887-5903.
- X.-Q. Wu, J. Zhao, Y.-P. Wu, W.-w. Dong, D.-S. Li, J.-R. Li and Q. Zhang, *ACS Appl. Mater. Interfaces*, 2018, **10**, 12740-12749.
- S. Gu, J. He, Y. Zhu, Z. Wang, D. Chen, G. Yu, C. Pan, J. Guan and K. Tao, *ACS Appl. Mater. Interfaces*, 2016, **8**, 18383-18392.
- S. Zhang, K. Dokko and M. Watanabe, *Mater. Horiz.*, 2015, **2**, 168-197.
- J. S. Lee, X. Wang, H. Luo, G. A. Baker and S. Dai, *J. Am. Chem. Soc.*, 2009, **131**, 4596-4597.
- N. Fechner, T.-P. Fellinger and M. Antonietti, *Adv. Mater.*, 2013, **25**, 75-79.
- X. Kang, X. Sun and B. Han, *Adv. Mater.*, 2016, **28**, 1011-1030.
- M. Watanabe, M. L. Thomas, S. Zhang, K. Ueno, T. Yasuda and K. Dokko, *Chem. Rev.*, 2017, **117**, 7190-7239.
- Q. Yang, Z. Zhang, X.-G. Sun, Y.-S. Hu, H. Xing and S. Dai, *Chem. Soc. Rev.*, 2018, **47**, 2020-2064.
- Y. Deng, Y. Xie, K. Zou and X. Ji, *J. Mater. Chem. A*, 2016, **4**, 1144-1173.
- J. Zhang, L. Qu, G. Shi, J. Liu, J. Chen and L. Dai, *Angew. Chem.-Int. Edit.*, 2016, **55**, 2230-2234.
- Y. Ding, X. Huang, X. Yi, Y. Qiao, X. Sun, A. Zheng and D. S. Su, *Angew. Chem.-Int. Edit.*, 2018, **57**, 13800-13804.
- W. Yang, T.-P. Fellinger and M. Antonietti, *J. Am. Chem. Soc.*, 2011, **133**, 206-209.
- J. P. Paraknowitsch, J. Zhang, D. Su, A. Thomas and M. Antonietti, *Adv. Mater.*, 2010, **22**, 87-92.
- J. S. Lee, X. Wang, H. Luo and S. Dai, *Adv. Mater.*, 2010, **22**, 1004-1007.
- S. Zhang, M. S. Miran, A. Ikoma, K. Dokko and M. Watanabe, *J. Am. Chem. Soc.*, 2014, **136**, 1690-1693.
- L. Sun, Y. Yao, Y. Zhou, L. Li, H. Zhou, M. Guo, S. Liu, C. Feng, Z. Qi and B. Gao, *ACS Sustain. Chem. Eng.*, 2018, **6**, 13494-13503.
- H. Zhou, Y. Zhou, L. Li, Y. Li, X. Liu, P. Zhao and B. Gao, *ACS Sustain. Chem. Eng.*, 2019, **7**, 9281-9290.
- J. S. Lee, H. Luo, G. A. Baker and S. Dai, *Chem. Mater.*, 2009, **21**, 4756-4758.
- X. Zhu, C. Tian, S. M. Mahurin, S.-H. Chai, C. Wang, S. Brown, G. M. Veith, H. Luo, H. Liu and S. Dai, *J. Am. Chem. Soc.*, 2012, **134**, 10478-10484.
- Y. Su, H. Wang, J. Zhao, M. H. Rummeli, Y. Gao, Y.-B. Jiang, L. Zhang and G. Zou, *Electrochim. Acta*, 2018, **280**, 258-265.
- G. Chen, X. Wang, J. Li, W. Hou, Y. Zhou and J. Wang, *ACS Appl. Mater. Interfaces*, 2015, **7**, 18508-18518.
- L. Hu, J. Hou, Y. Ma, H. Li and T. Zhai, *J. Mater. Chem. A*, 2016, **4**, 15006-15014.
- D. Wu, J. Cheng, T. Wang, P. Liu, L. Yang and D. Jia, *ACS Sustain. Chem. Eng.*, 2019, **7**, 12138-12147.
- Z. Yang, S. Wang, Z. Zhang, W. Guo, K. Jie, M. I. Hashim, O. Š. Miljanić, D.-e. Jiang, I. Popovs and S. Dai, *J. Mater. Chem. A*, 2019, **7**, 17277-17282.
- T. Shi, Y. Zheng, T. Wang, P. Li, Y. Wang and D. Yao, *ChemPhysChem*, 2018, **19**, 130-137.
- Y. Zhao, K. X. Yao, B. Teng, T. Zhang and Y. Han, *Energy Environ. Sci.*, 2013, **6**, 3684-3692.

- 40 S. Sircar, T. C. Golden and M. B. Rao, *Carbon*, 1996, **34**, 1-12.
- 41 M. R. Liebl and J. Senker, *Chem. Mater.*, 2013, **25**, 970-980.
- 42 R. Dawson, D. J. Adams and A. I. Cooper, *Chem. Sci.*, 2011, **2**, 1173-1177.
- 43 A. Laybourn, R. Dawson, R. Clowes, J. A. Iggo, A. I. Cooper, Y. Z. Khimiyak and D. J. Adams, *Polym. Chem.*, 2012, **3**, 533-537.
- 44 W. Lu, D. Yuan, J. Sculley, D. Zhao, R. Krishna and H.-C. Zhou, *J. Am. Chem. Soc.*, 2011, **133**, 18126-18129.
- 45 M. Saleh, J. N. Tiwari, K. C. Kemp, M. Yousuf and K. S. Kim, *Environ. Sci. Technol.*, 2013, **47**, 5467-5473.
- 46 M. Saleh, H. M. Lee, K. C. Kemp and K. S. Kim, *ACS Appl. Mater. Interfaces*, 2014, **6**, 7325-7333.
- 47 L. Shao, M. Liu, J. Huang and Y.-N. Liu, *J. Colloid Interf. Sci.*, 2018, **513**, 304-313.
- 48 M. Liu, L. Shao, J. Huang and Y.-N. Liu, *Microporous Mesoporous Mater.*, 2018, **264**, 104-111.
- 49 P. Samanta, P. Chandra, S. Dutta, Aamod V. Desai and S. K. Ghosh, *Chem. Sci.*, 2018, **9**, 7874-7881.
- 50 P. Arab, E. Parrish, T. İslamoğlu and H. M. El-Kaderi, *J. Mater. Chem. A*, 2015, **3**, 20586-20594.
- 51 C. Zhang, P.-C. Zhu, L. Tan, J.-M. Liu, B. Tan, X.-L. Yang and H.-B. Xu, *Macromolecules*, 2015, **48**, 8509-8514.
- 52 F. Niu, L. Tao, Y. Deng, H. Gao, J. Liu and W. Song, *New J. Chem.*, 2014, **38**, 5695-5699.
- 53 J. Byun, H. A. Patel, D. Thirion and C. T. Yavuz, *Nat. Commun.*, 2016, **7**, 13377-13387.